Supporting Information

DFT investigation of oxygen reduction reaction on nitrogen (N) doped graphdiyne as an electrocatalyst: the importance of pre-adsorbed OH* and solvation effect

Yuelin Wang[a], Thanh Ngoc Pham[a], Harry H. Halim[a], Likai Yan[c], Yoshitada Morikawa[a,b*]

[a]*Department of Precision Engineering, Graduate School of Engineering, Osaka University, 2-1, Yamada-oka, Suita, Osaka 565-0871, Japan*

[b]*Research Center for Precision Engineering, Graduate School of Engineering, Osaka University, 2-1 Yamada-oka, Suita 565-0871, Osaka, Japan*

[c]*Institute of Functional Material Chemistry, Key Laboratory of Polyoxometalate Science of Ministry of Education, Faculty of Chemistry, Northeast Normal University, Changchun 130024, P. R. China*

Corresponding author: morikawa@prec.eng.osaka-u.ac.jp

Free energy calculation

The ORR mechanism is divided into dissociative mechanism and associative mechanism. For the dissociative mechanism, ORR proceeds with the following elementary steps[1-2]:

$$O_2\,(g) + * \rightarrow 2O* \quad (1)$$

$$2O*+H_2O(l)+e^- \rightarrow O*+ OH*+OH^- \quad (2)$$

$$O*+OH*+ e^- \rightarrow O*+ OH^- \quad (3)$$

$$O*+ H_2O(l)+ e^- \rightarrow OH*+ OH^- \quad (4)$$

$$OH*+ e^- \rightarrow OH^-+* \quad (5)$$

The associative mechanism proceeds as follows[1-2]:

$$O_2\,(g)+ H_2O(l)+ e^- + * \rightarrow OOH*+OH^- \quad (6)$$

$$OOH*+ e^- \rightarrow O*+ OH^- \quad (7)$$

$$O*+ H_2O(l)+ e^{-\cdot} \rightarrow OH*+ OH^- \quad (4)$$

$$OH*+ e^- \rightarrow OH^-+* \quad (5)$$

The reaction Gibbs free energies (ΔG) of the reactions (1)–(7) can be expressed as:

$$\Delta G_1 = \mu_{2O*} - \mu_{O_2} - \mu_* \quad (8)$$

$$\Delta G_2 = \mu_{O*+OH*} + \mu_{OH^-} - (\mu_{2O*} + \mu_{H_2O(l)} + \mu_e-) \quad (9)$$

$$\Delta G_3 = \mu_{O*} + \mu_{OH^-} - (\mu_{O*+OH*} + \mu_e-) \quad (10)$$

$$\Delta G_4 = \mu_{OH*} + \mu_{OH^-} - (\mu_{O*} + \mu_{H_2O(l)} + \mu_e-) \quad (11)$$

$$\Delta G_5 = \mu_* + \mu_{OH^-} - (\mu_{OH*} + \mu_e-) \quad (12)$$

$$\Delta G_6 = \mu_{OOH*} + \mu_{OH^-} - (\mu_{O_2}+\mu_* + \mu_{H_2O(l)} + \mu_e-) \quad (13)$$

$$\Delta G_7 = \mu_{O*} + \mu_{OH^-} - (\mu_{OOH*} + \mu_e-) \quad (14)$$

where μ denotes the (electro)chemical potential of the indicated species. These chemical potentials of the reaction intermediates can be obtained from[3]:

$$\mu_* = E_* \quad (15)$$

$$\mu_{X*} = E_{X*} + H_{X*} - TS_{X*} \quad (16)$$

$$\mu_{H_2O(l)} = E_{H_2O(l)} + H_{H_2O(l)} - TS_{H_2O(l)} = E_{H_2O(g)} + H_{H_2O(g)} - TS_{H_2O(g)} + RT \times \ln\left(\frac{P}{P_0}\right) \quad (17)$$

$$H = E_{elec} + E_{ZPE} + \int_0^T C_P dT \quad (18)$$

where E_* and E_{X*} are the (DFT) total energies of the clean surface ($*$) and of surfaces with a single adsorbed species X, respectively. H_{X*}, S_{X*} are the corresponding enthalpies and entropies, respectively. T is the temperature (298.15 K). $E_{H_2O(g)}$, $H_{H_2O(g)}$ and $S_{H_2O(g)}$ are the DFT total energy, enthalpy and entropy of gas H_2O, respectively. Enthalpies and entropies for gas phase molecules have been determined in the ideal gas limit[4]; for adsorbates, the harmonic limit was used[5]. The chemical potential for H_2O (g) is calculated at 0.035 bar[6] because this is the equilibrium pressure of H_2O (l) at 298.15 K. R is gas constant, P_0 with = 1 bar, and P = 0.035 bar. For O_2, the chemical potential is obtained from the experimental formation energy of O_2 with respect to water, because DFT tends to underestimate the O_2 atomization energy. According to the thermodynamic energy (4.92 eV) released by the reaction of $2H_2$ (g) + O_2 (g) → $2H_2O$ (l) can be written as[6]:

$$\mu_{O_2(g)} = 2\mu_{H_2O(l)} + 4.92 - 2\mu_{H_2(g)} \quad (19)$$

For μ_{OH^-} and μ_{e^-}, we only need the difference $\mu_{OH^-} - \mu_{e^-}$. To calculate this difference, we assume the equilibrium H_2O (l) ↔ H^+ + OH^-, which relates the chemical potentials as:

$$\mu_{OH^-} + \mu_{H^+} = \mu_{H_2O(l)} \quad (20)$$

rewritten as：

$$\mu_{OH^-} - \mu_{e^-} + \mu_{H^+} + \mu_{e^-} = \mu_{H_2O(l)} \quad (21)$$

$$\mu_{OH^-} - \mu_{e^-} = \mu_{H_2O(l)} - (\mu_{H^+} + \mu_{e^-}) \quad (22)$$

Here, ($\mu_{H^+} + \mu_{e^-}$) can be calculated using the computational hydrogen (CHE) approach ($H^+ + e^- \leftrightarrow$ ½H_2 (g))[7], so the chemical potential of $\mu_{H^+} + \mu_{e^-}$ can be calculated using:

$$\mu_{H^+} + \mu_{e^-} = 1/2\mu_{H_2} \quad (23)$$

We describe this equilibrium using the reversible hydrogen electrode (RHE)[8] as the reference electrode, which it equals the chemical potential of $H^+ + e^-$ to the chemical potential of $1/2H_2$ at arbitrary pH (pH_2 = 1 bar and T = 298.15 K), so μ_{H^+} and μ_{e^-} can be expressed as:

$$\mu_{H^+} = \mu_{H^+}^{RHE} \quad (24)$$

$$\mu_{e^-} = \mu_{e^-}^{RHE} - eU_{RHE} \quad (25)$$

where U_{RHE} is the potential of the electrode relative to the RHE.

Combining equations (23)–(25), the equilibrium can be expressed as:

$$\mu_{H^+} + \mu_{e^-} = \mu_{H^+}^{RHE} + \mu_{e^-}^{RHE} - eU_{RHE} = 1/2\mu_{H_2} - eU_{RHE} \quad (26)$$

Substituting the equation (26) into equation (22) to obtain the following equation:

$$\mu_{OH^-} - \mu_{e^-} = \mu_{H_2O(l)} - (1/2\mu_{H_2} - eU_{RHE}) \quad (27)$$

Using equation (27) to replace the term ($\mu_{OH^-} - \mu_{e^-}$) in equations, we finally get the reaction Gibbs free energies:

$$\Delta G_1 = \mu_{2O*} - 2\mu_{H_2O(l)} - 4.92 + 2\mu_{H_2} - E_* \quad (28)$$

$$\Delta G_2 = \mu_{O*+OH*} - \mu_{2O*} - 1/2\mu_{H_2} + eU_{RHE} \quad (29)$$

$$\Delta G_3 = \mu_{O*} - \mu_{O*+OH*} + \mu_{H_2O(l)} - 1/2\mu_{H_2} + eU_{RHE} \quad (30)$$

$$\Delta G_4 = \mu_{OH*} - \mu_{O*} - 1/2\mu_{H_2} + eU_{RHE} \quad (31)$$

$$\Delta G_5 = \mu_{*} - \mu_{OH*} + \mu_{H_2O(l)} - 1/2\mu_{H_2} + eU_{RHE} \quad (32)$$

$$\Delta G_6 = \mu_{OOH*} - E_* - 2\mu_{H_2O(l)} - 4.92 + 3/2\mu_{H_2} + eU_{RHE} \quad (33)$$

$$\Delta G_7 = \mu_{O*} - \mu_{OOH*} + \mu_{H_2O(l)} - 1/2\mu_{H_2} + eU_{RHE} \quad (34)$$

The overpotential is given by:

$$\eta = \frac{1}{e}\Delta G_{max} + 1.23 \tag{35}$$

In our work, we also consider solvation energy ΔSol(X*) defined by the energy difference between the ΔE of 2O*, O*+OH*, OOH, O* and *OH on the surface with and without water and the equation as follow[9]:

$$\Delta Sol(X^*) = \Delta E_{X^*+mH_2O^*} - \Delta E_{X^*} \tag{36}$$

Where $\Delta E_{X^*+mH_2O}$, ΔE_{X^*} are the adsorption energies change of each intermediate on surface with and without water, defined as follows[9]:

$$\Delta E_{2O^*+mH_2O^*} = E_{2O^*+mH_2O^*} - E_* - m\Delta E_{nH_2O^*} - mE_{H_2O(g)} - [2E_{H_2O(g)} - 2E_{H_2}] \tag{37}$$

$$\Delta E_{O^*+OH^*+mH_2O^*} = E_{O^*+OH^*+mH_2O^*} - E_* - m\Delta E_{nH_2O^*} - mE_{H_2O(g)} - [2E_{H_2O(g)} - 3/2E_{H_2}] \tag{38}$$

$$\Delta E_{OOH^*+mH_2O^*} = E_{OOH^*+mH_2O^*} - E_* - m\Delta E_{nH_2O^*} - mE_{H_2O(g)} - [2E_{H_2O(g)} - 3/2E_{H_2}] \tag{39}$$

$$\Delta E_{O^*+mH_2O^*} = E_{O^*+mH_2O^*} - E_* - m\Delta E_{nH_2O^*} - mE_{H_2O(g)} - [E_{H_2O(g)} - E_{H_2}] \tag{40}$$

$$\Delta E_{OH^*+mH_2O^*} = E_{OH^*+mH_2O^*} - E_* - m\Delta E_{nH_2O^*} - mE_{H_2O(g)} - [E_{H_2O(g)} - 1/2E_{H_2}] \tag{41}$$

$$\Delta E_{2O^*} = E_{2O^*} - E_* - [2E_{H_2O(g)} - 2E_{H_2}] \tag{42}$$

$$\Delta E_{O^*-OH^*} = E_{O^*-OH^*} - E_* - [2E_{H_2O(g)} - 3/2E_{H_2}] \tag{43}$$

$$\Delta E_{OOH^*} = E_{OOH^*} - E_* - [2E_{H_2O(g)} - 3/2E_{H_2}] \tag{44}$$

$$\Delta E_{O^*} = E_{O^*} - E_* - [E_{H_2O(g)} - E_{H_2}] \tag{45}$$

$$\Delta E_{OH^*} = E_{OH^*} - E_* - [E_{H_2O(g)} - 1/2E_{H_2}] \tag{46}$$

Where $E_{2O^*+mH_2O^*}$, $E_{O^*-OH^*+mH_2O^*}$, $E_{OOH^*+mH_2O^*}$, $E_{O^*+mH_2O^*}$, $E_{OH^*+mH_2O^*}$, E_{2O^*}, $E_{O^*-OH^*}$, E_{OOH^*}, E_{O^*} and E_{OH^*} are total energy of 2O*, O*+OH*, OOH, O* and *OH on surface with and without water, n is the number of water molecules in water layer, m = n−1, $\Delta E_{nH_2O^*}$ is[9]:

$$\Delta E_{nH_2O^*} = (E_{nH_2O^*} - E_* - nE_{H_2O(g)})/n \tag{47}$$

Finally, the adsorption free energy of each ORR intermediates including the solvation effect was defined as:

$$\Delta G_{\text{ads}}(\text{X}^*) = \Delta E_{\text{X}*} + (\Delta H_{\text{X}*} - T\Delta \text{S}_{\text{X}*}) - neU_{\text{RHE}} + \Delta\text{Sol}(\text{X}^*) \quad (48)$$

AIMD set-up

To elucidate the effect of solvents on the ORR mechanism, we calculated the *ab inito* molecular dynamics (AIMD)[10] employing the "effective screening medium" method[11] by using STATE. Representative of the configurational simulation cells is shown in Scheme S1. A semi-infinite continuum with an infinite dielectric constant, i.e., a classical conductor, was located beyond $Z = Z_1$, while another region was characterized by the dielectric constant of unity, i.e., the vacuum medium. The neutral charge is introduced in this work. An artificial boundary (Z_2 = 9.3 Å) was placed above the surface and water molecules, restricting their movement, and maintaining the density at ~1 g/cm^3. In Scheme S1, $Z_3<Z<Z_2$ region is the contact region of water with vacuum, $Z_4<Z<Z_3$ is the "bulk" water region where it corresponds to regions around 1 g/cm^3 of the experimental bulk water density, and $Z_5<Z<Z_4$ is water contact region with the surface. The AIMD simulations were sampled by the canonical (NVT) ensemble employing Nose-Hoover thermostats with a time step of 1.0 fs at a finite temperature of 400 K. We chose 400 K which is higher than the experiment condition (~300K), this is due to overestimation of the melting point of ice predicted by DFT[12]. Moreover, higher temperature also helps us explore more local minimum structures of water/NGDY interfaces. Upon these systems, we performed 18 ps long AIMD simulations with the last 15 ps used for analysis. Then, we chose the five snapshots with the most hydrogen bond (H bond) networks in the contact region with the surface ($Z_5<Z<Z_4$) within the last 15 ps. Finally, we replace one water that is near the active site with the ORR intermediate and use equation (35)-(45) to get the average solvation energy (ΔSol*)* of each ORR intermediate.

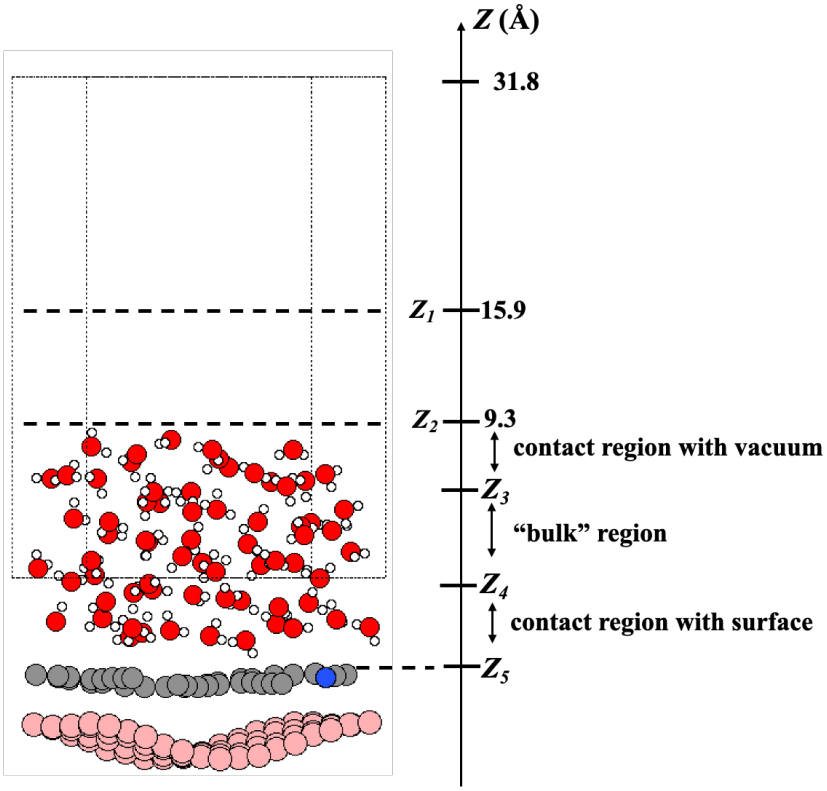

Scheme S1 Computational set-up of the simulation (e.g. one snapshot of sp-N1GDY/G). Red, white, gray, pink, and blue balls are O atoms, H atoms, C atoms in N-doped GDY, C atoms in G, and N atoms, respectively.

Table S1 Band gap (E_g) of corrugated graphene (G), GDY, N (sp-N1, sp-N2, Pyri-N)-doped GDY, N (sp-N1, sp-N2, Pyri-N) doped GDY/G were calculated by the PBE and HSE06 functional.

	E_g (eV)		
	PBE	HSE06	Ref.
corrugated G	zero-gap semiconductor	zero-gap semiconductor	—
GDY	0.5	0.9	0.89 (HES06)[13] /1.10 (GW)[14]
sp-N1GDY	metallic	metallic	metallic[15]
sp-N2GDY	metallic	metallic	—
Pyri-NGDY	0.6	0.97	—
sp-N1GDY/G	metallic	metallic	—
sp-N2GDY/G	metallic	metallic	—
Pyri-NGDY/G	metallic	metallic	—

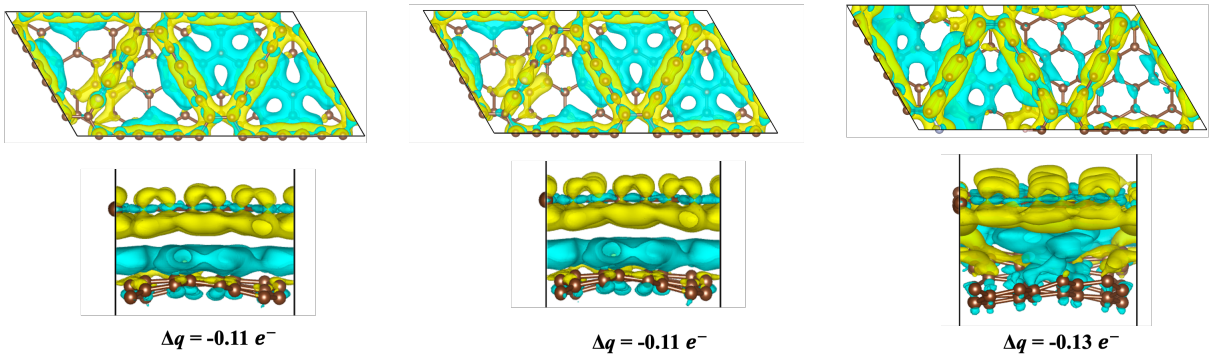

Figure S1 The top view and side view of CDD on sp-N1GDY/G (a), sp-N2GDY/G (b), and Pyri-NGDY/G (c), the yellow, and blue isosurfaces represent charge accumulation and depletion, respectively. The isosurface value is around 0.00018 e/Å^3. Bader charge of three N-doped GDY/G is listed in which $\Delta q = Z - q$, where Z is the total valence electrons of atoms (1, 4, and 5 for H, C, and N, respectively) and q is the total Bader electrons.

Table S2 The calculated work function of planar graphene, corrugated graphene, GDY, sp-N1GDY, sp-N2GDY, Pyri-NGDY, sp-N1GDY/G, sp-N2GDY/G, and Pyri-NGDY/G.

	work function	Ref.
planar graphene	4.20 eV	4.25 eV[16], 4.38 eV[17], 4.50 eV (Exp.)[18]
corrugated graphene	4.10 eV	—
GDY	5.10 eV	5.13 eV[19], 6.0 eV (Exp.)[19]
sp-N1GDY	4.53 eV	—
sp-N2GDY	4.53 eV	—
Pyri-NGDY	4.93 eV	—
sp-N1GDY/G	4.40 eV	—
sp-N2GDY/G	4.40 eV	—
Pyri-NGDY/G	4.62 eV	—

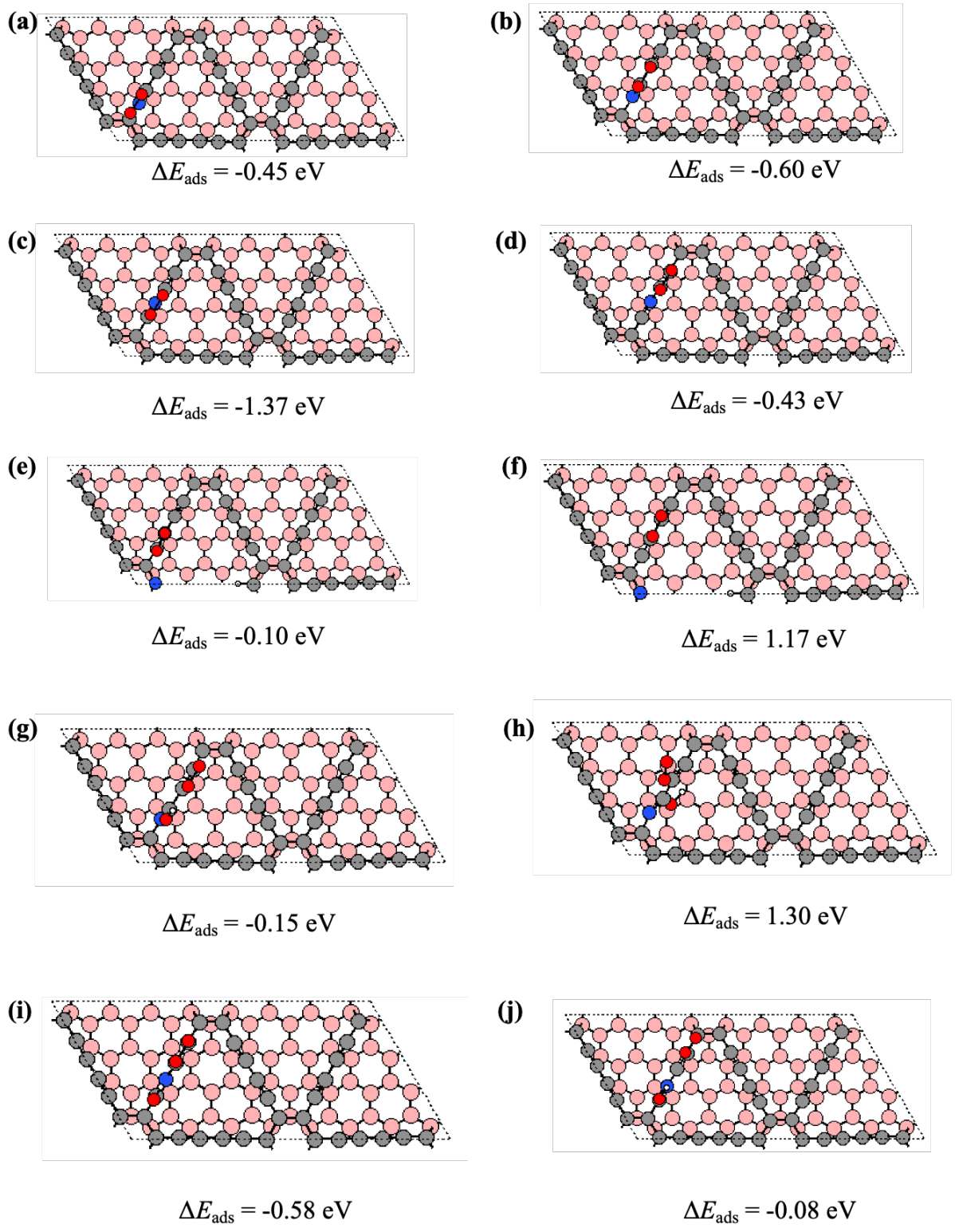

Figure S2 The possible active sites of O_2 absorption on sp-N1GDY/G (a,b), on sp-N2GDY/G (c, d), and on Pyri-NGDY/G (e, f), sp-N1GDY(OH)/G (g, h), on sp-N2GDY(OH)/G (i, j). Red, white, gray, pink, and blue balls are O atoms, H atoms, C atoms in N-doped GDY, C atoms in G, and N atoms, respectively.

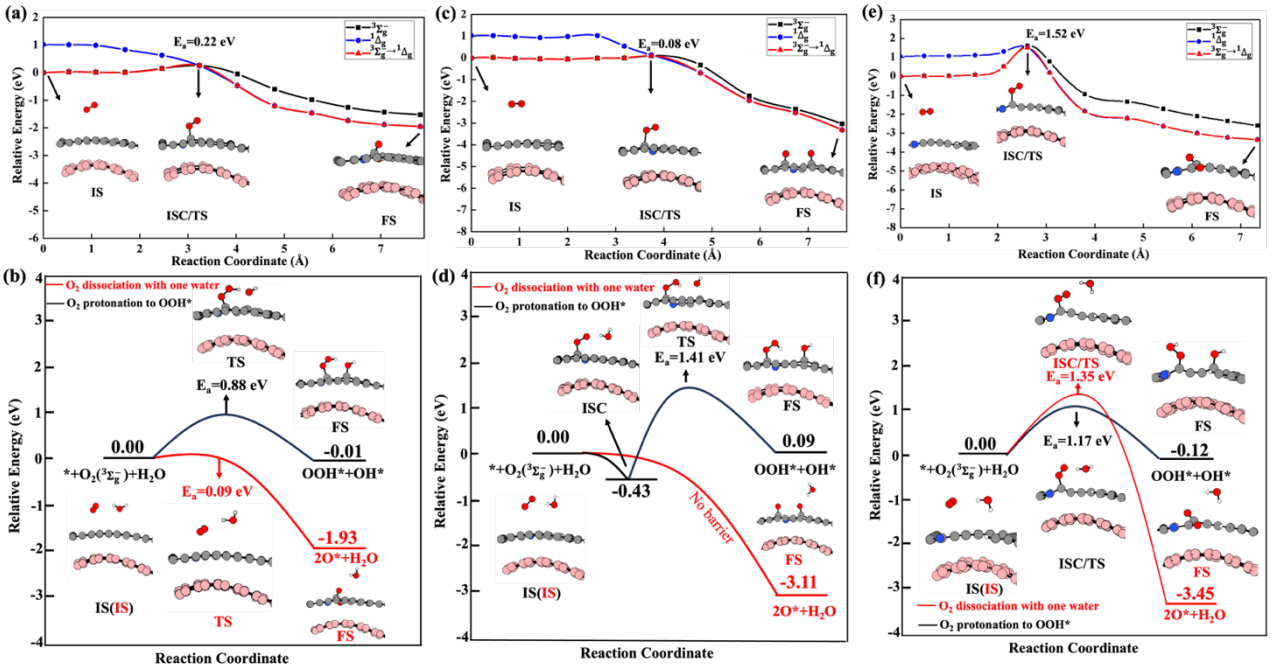

Figure S3 Reaction path of (a) O_2 dissociation, (b) O_2 protonation to OOH* and O_2 dissociation with one H_2O on sp-N1GDY/G. Reaction path of (c) O_2 dissociation, (d) O_2 protonation to OOH* and O_2 dissociation with one H_2O on sp-N2GDY/G. Reaction path of (e) O_2 dissociation, (f) O_2 protonation to OOH* and O_2 dissociation with one H_2O on Pyri-NGDY/G. Structures corresponding to the initial state (IS), intersystem crossing state/transition state (ISC/TS), and final state (FS) are shown. Red, white, gray, pink, and blue balls are O atoms, H atoms, C atoms in N-doped GDY, C atoms in G, and N atoms, respectively.

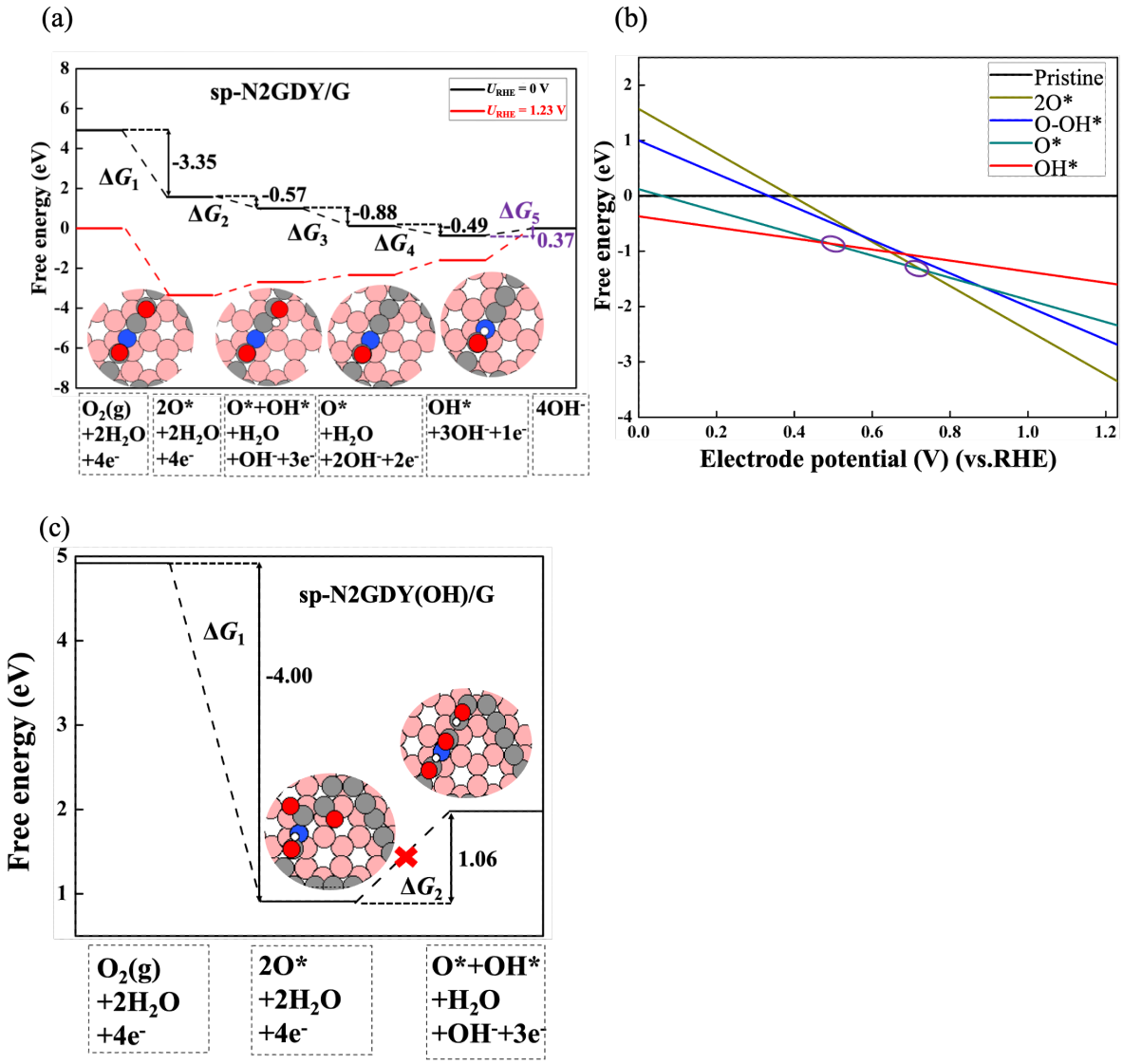

Figure S4 Free energy diagram (a) and structures of each ORR intermediate on sp-N2GDY/G and (b) free energy of each ORR intermediate versus electrode potential (vs. RHE) on sp-N2GDY/G; Free energy diagram and structures (c) of ORR intermediates on sp-N2GDY(OH)/G. Red, white, gray, pink, and blue balls are O atoms, H atoms, C atoms in N-doped GDY, C atoms in G, and N atoms, respectively.

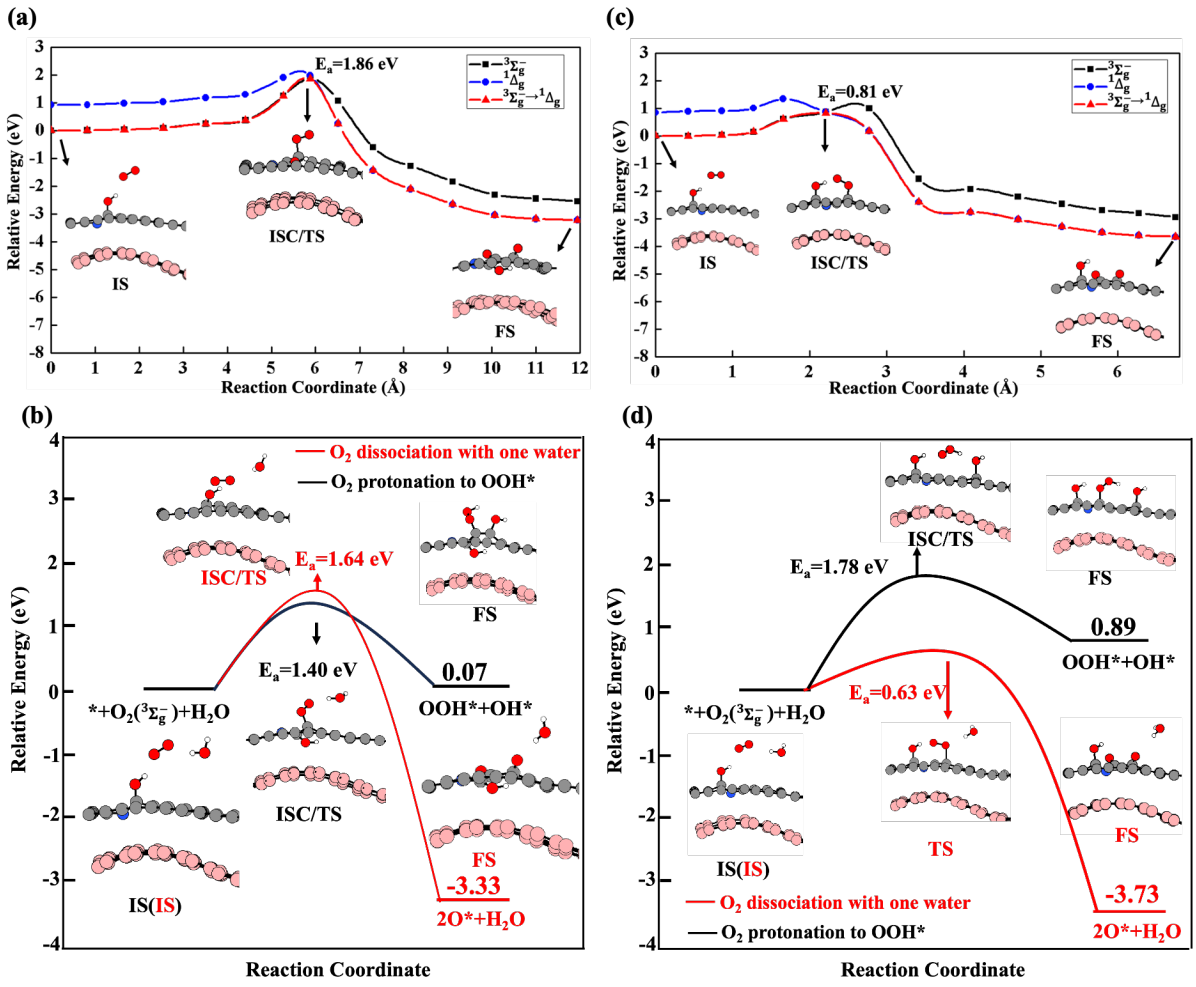

Figure S5 Reaction path of (a) O_2 dissociation, (b) O_2 protonation to OOH* and O_2 dissociation with one H_2O on sp-N1GDY(OH)/G. Reaction path of (c) O_2 dissociation, (d) O_2 protonation to OOH* and O_2 dissociation with one H_2O on sp-N2GDY(OH)/G. Structures corresponding to the initial state (IS), intersystem crossing state/transition state (ISC/TS), and final state (FS) are shown. Red, white, gray, pink, and blue are O atom, H atom, C atom in N-doped GDY, C atom in G, and N atom, respectively.

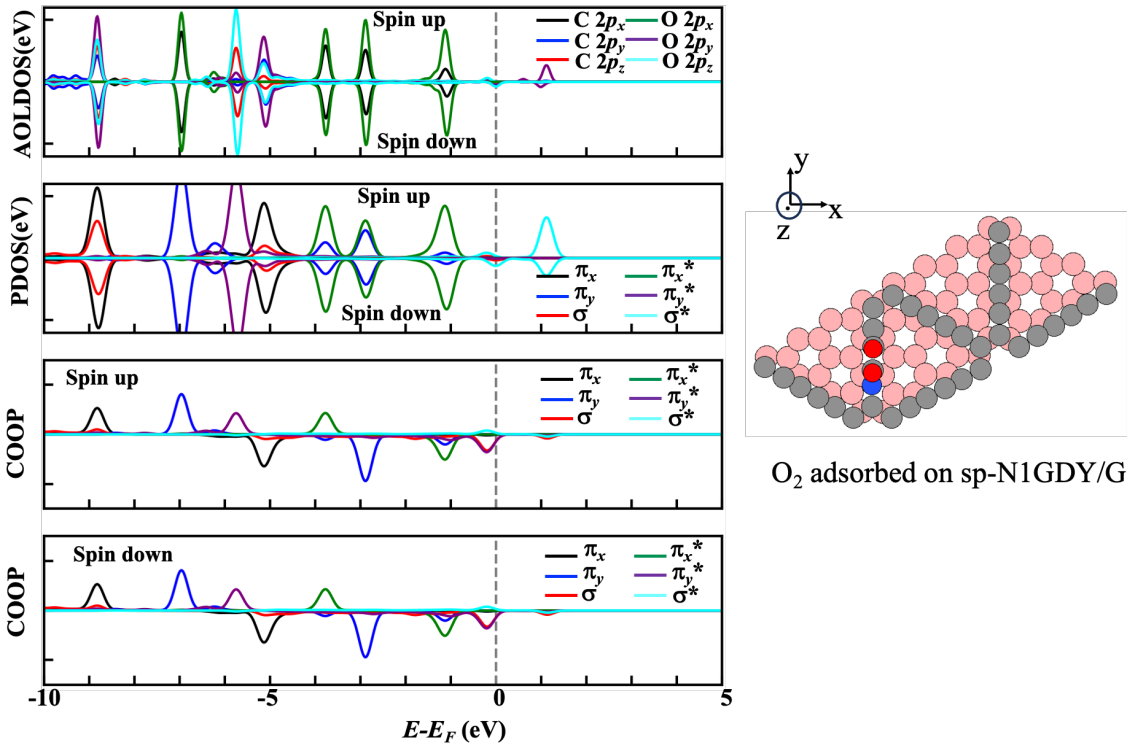

Figure S6 The atomic orbital local density of states (AOLDOS), projected density of states into crystal orbitals (PDOS) and crystal orbital overlap population (COOP) of O_2 adsorbed on sp-N1GDY/G.

Table S3 Adsorption energy (ΔE_{ads}/eV) of each ORR intermediate on each surface and distance (d/Å) between O_2 and surface in vacuum.

	ΔE_{ads} (O_2)	d	ΔE_{ads} (2O)	ΔE_{ads} (O+OH)	ΔE_{ads} (OOH)	ΔE_{ads} (O)	ΔE_{ads} (OH)	ΔE_{ads} (H_2O)
sp-N1GDY/G	-0.60	1.425	-11.71	-9.56	—	-6.05	-4.08	-0.11
sp-N1GDY(OH)/G	-0.15	3.074	—	—	-1.23	-4.97	-2.86	-0.09
sp-N2GDY/G	-1.37	1.368	-12.81	-10.17	—	-7.08	-4.36	-0.18
sp-N2GDY(OH)/G	-0.58	1.426	-13.47	—	—	—	—	—
Pyri-NGDY/G	-0.10	3.100	—	—	-0.93	-4.98	-2.52	-0.06

Table S4 The calculated E_{ZPE}, TS, and $\int_0^T C_P dT$ of gas-phase molecules and each ORR intermediate.

	E_{ZPE}/eV	TS/eV	$\int_0^T C_P dT$/eV
2O*	0.18	0.11	0.061
O*+OH*	0.49	0.11	0.062
OOH*	0.45	0.18	0.086
O*	0.10	0.05	0.026
OH*	0.40	0.06	0.037
H_2O (g)	0.56	0.58	0.106
H_2 (g)	0.27	0.43	0.091

Table S5 Reaction Gibbs free energy of each ORR intermediate on sp-N1GDY/G, sp-N1GDY(OH)/G and Pyri-NGDY with and without water; reaction Gibbs free energy of ORR on sp-N2GDY/G and sp-N2GDY(OH)/G without water.

	ΔG_1	ΔG_2	ΔG_3	ΔG_4	ΔG_5	ΔG_6	ΔG_7
sp-N1GDY/G	-2.24	-1.07	-0.88	-0.86	0.13	—	—
sp-N1GDY/G with water	-2.49	-1.07	-0.89	-0.85	0.38	—	—
sp-N1GDY(OH)/G	—	—	—	-1.08	-1.15	-0.51	-2.18
sp-N1GDY(OH)/G with water	—	—	—	-1.07	-0.90	-0.77	-2.18
sp-N2GDY/G	-3.35	-0.57	-0.88	-0.49	0.37	—	—
sp-N2GDY(OH)/G	-4.00	1.06(×)	—	—	—	—	—
Pyri-NGDY	—	—	—	-0.74	-1.47	-0.22	-2.49
Pyri-NGDY with water	—	—	—	-0.52	-1.29	-0.48	-2.63

Table S6 Adsorption Gibbs free energy of each ORR intermediate on sp-N1GDY, sp-N2GDY, sp-N2GDY/G, sp-N2GDY(OH)/G, and Pyri-NGDY without water; sp-N1GDY/G, sp-N1GDY(OH)/G, Pyri-NGDY/G, and Pyri-NGDY/G with and without water.

	ΔG_{ads} (2O*)	ΔG_{ads} (O*+OH*)	ΔG_{ads} (OOH*)	ΔG_{ads} (O*)	ΔG_{ads} (OH*)
sp-N1GDY	2.82	1.63	—	0.91	-0.10
sp-N1GDY/G	2.68	1.61	—	0.73	-0.13
sp-N1GDY/G with water	2.43	1.36	—	0.47	-0.38
sp-N1GDY(OH)	—	—	4.44	2.26	1.17
sp-N1GDY(OH)/G	—	—	4.41	2.23	1.15
sp-N1GDY(OH)/G with water	—	—	4.15	1.97	0.90
sp-N2GDY	1.71	1.13	—	0.48	-0.31
sp-N2GDY/G	1.57	1.00	—	0.12	-0.37
sp-N2GDY(OH)/G	0.92	1.98(×)	—	—	—
Pyri-NGDY	—	—	4.86	2.41	1.59
Pyri-NGDY/G	—	—	4.70	2.21	1.47
Pyri-NGDY/G with water	—	—	4.44	1.81	1.29

AIMD analysis:

To distinguish the water region, the average density profiles of H_2O (ρ) as a function of Z position on the sp-N1GDY/G (Figure S7a) and Pyri-NGDY/G (Figure S7b) are shown in Figure 7. In both cases, the first sharply density peak of ρ is located at c.a. -3 Å (surface is located at c.a -6 Å) and extends up to -1 Å. Therefore, the region with -6.0 Å < Z < -1.0 Å is defined as the contact region between N-doped GDY and water solvents. The water density of the contact region is estimated to be around 1.4 $g \cdot cm^{-3}$, which is similar to that of the water/graphene interface surfaces[20]. Within the region of -1.0 Å < Z < 7.0 Å, water density oscillated and gradually decreased the bulk water density (~1.0 g/cm^3). Thus, we defined this region as the "bulk" water region. Above 7.0 Å until 9.3 Å (artificial boundary) appears another peak, called the water contact region with the vacuum. We mainly focus on the contact region with the surface (-6.0 Å < Z < -1.0 Å) to investigate the H bond networks.

Structural properties of water/N doped GDY are evaluated by radial distribution functions (RDF) and average coordination number (N_{OO}) of H_2O. We calculated and plotted the RDF(s) between oxygen atoms, R(r), and N_{OO} of the "bulk" region, and the contact layer with the surface on sp-N1GDY/G and Pyri-NGDY/G are shown in Figure S8 and Table S7. The RDF(s) curve and N_{OO} of the "bulk" region in both cases are similar to that obtained from the experiment at around 400 K[21-22]. The higher temperatures result in an overall softening of the structure, with diminishment of the first and second peaks, and a rise in the first minimum (r_{min}=3.6 Å) compared with that at room temperature (r_{min}=3.3 Å). We performed the average coordination number (N_{OO}) of H_2O in the contact region with the surface (-6.0 Å < Z < -1.0 Å) on both cases averaged over 5 ps (Figure S9). The results suggest that in 15 ps, the coordination number of water molecules is basically unchanged.

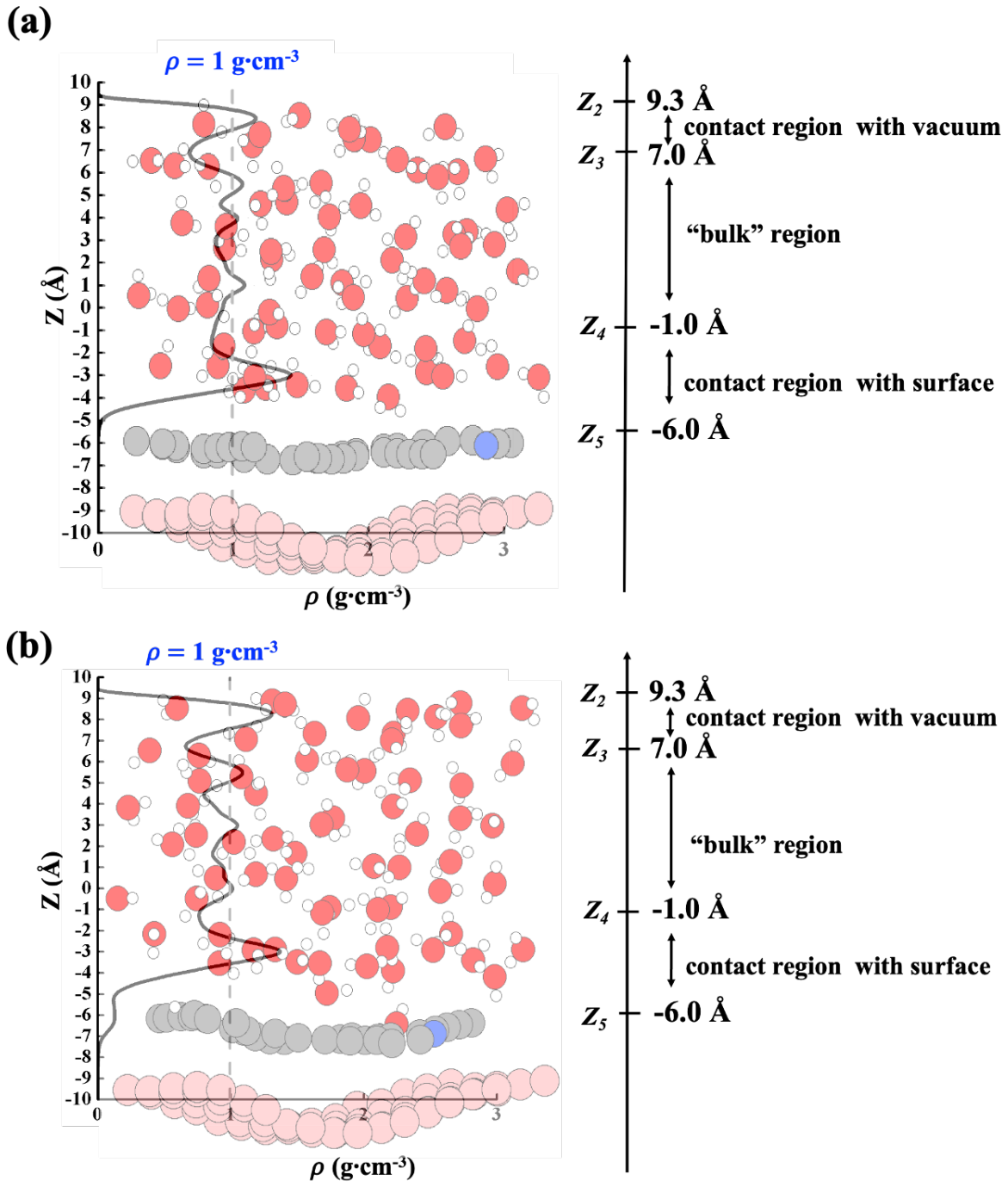

Figure S7 Calculated average density profile for the sp-N1GDY/G with water (a) and Pyri-NGDY/G with water (b) at 400 K. The gray solid line indicates the average atomic density and the gray dashed line indicates the density of bulk water (1 g·cm^{-3}). Red, white, gray, pink, and blue balls are O atoms, H atoms, C atoms in N-doped GDY, C atoms in G, and N atoms, respectively.

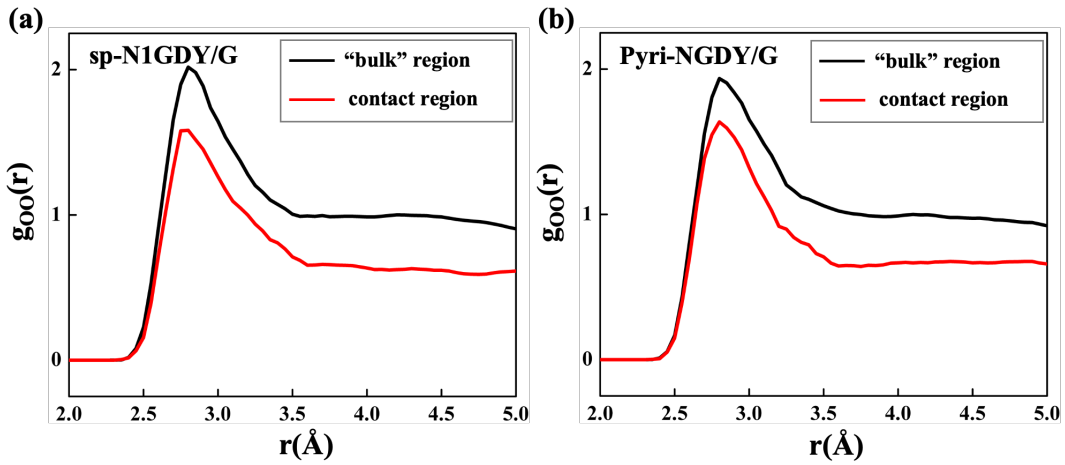

Figure S8 Oxygen-oxygen RDF(s) ($g_{OO}(r)$) for the "bulk" region (black line) and for the contact region with the surface (red line) on sp-N1GDY/G (a) and Pyri-NGDY/G (b).

Table S7 Coordination number N_{oo} of the contact layer and the "bulk" region, Temperature (*T*), the value of first minimum r_{min} in the $g_{OO}(r)$ of N-doped GDY/G compared with that of experiment values for bulk water.

	bulk water				contact region water			
	r_{max}	r_{min}	N_{OO}	*T*	r_{max}	r_{min}	N_{OO}	*T*
sp-N1GDY/G	2.8	3.6	5.30	400	2.8	3.6	4.06	400
Pyri-NGDY/G	2.8	3.6	5.27	400	2.8	3.6	4.08	400
experiment[15]	2.8	3.6	5.20	423	—	—	—	—

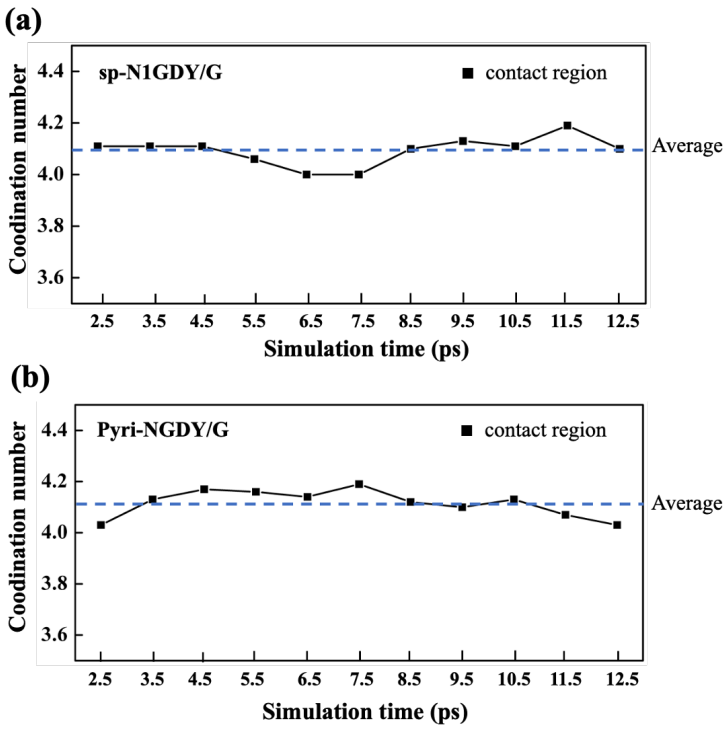

Figure S9 The average coordination number of H_2O in contact region with the surface (-6.0 Å < Z < -1.0 Å) on sp-N1GDY/G (a) and Pyri-NGDY/G (b) over a varying length of 5 ps.

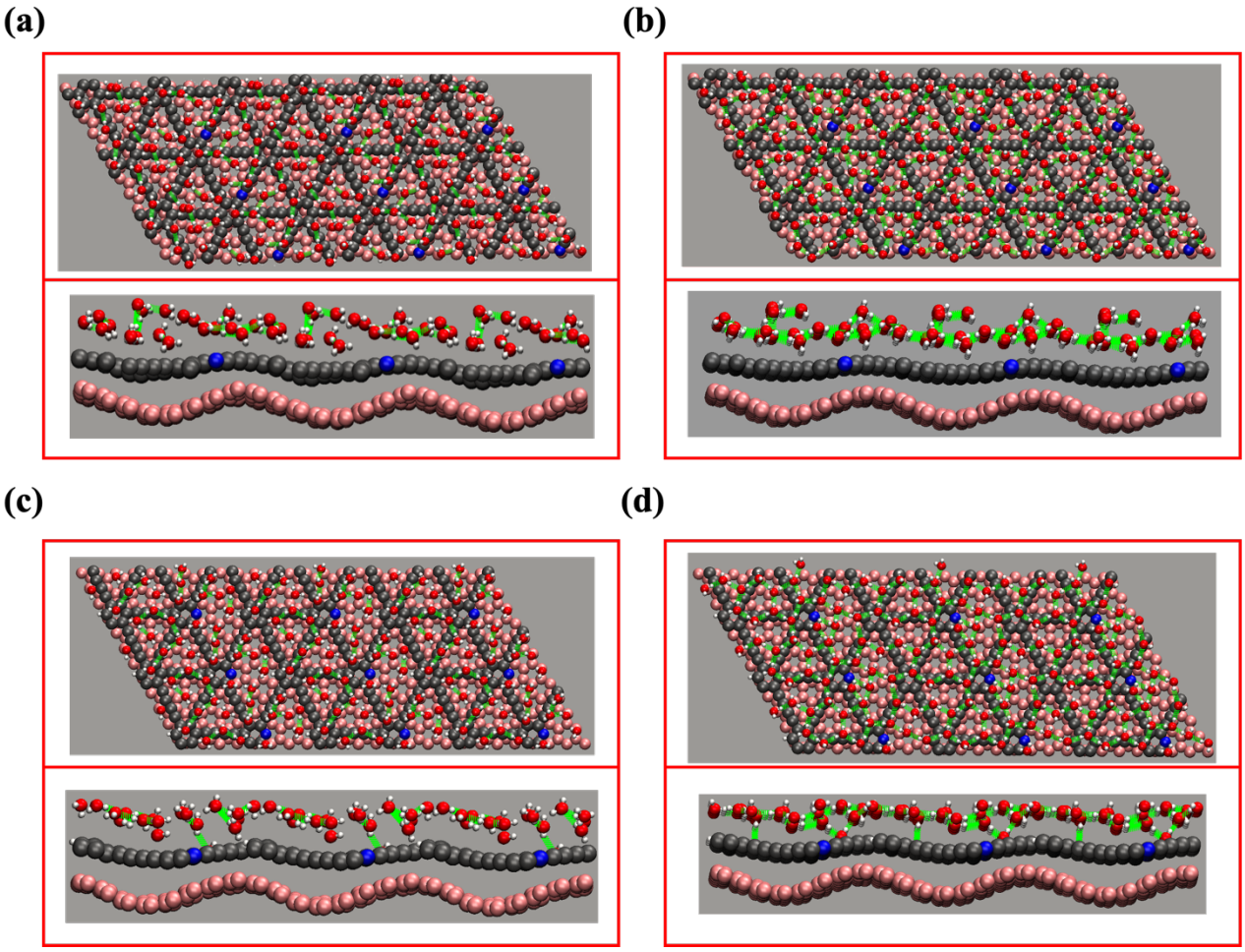

Figure S10 Top view (left) and side view (right) of H bond network on the sp-N1GDY/G in 400 K (a) and 0 K (b) and Pri-NGDY/G in 400 K (c) and 0 K (d) with 3x3 supercell. Red, white, gray, pink, and blue balls are O atoms, H atoms, C atoms in N-doped GDY, C atoms in G, and N atoms, respectively. The green dashed lines represent the H bond networks. We regard an H bond as being formed when the O–O distance of adjacent water molecules is smaller than 3.5 Å and the angle between the O–H vector of one molecule and the O–O vector is smaller than 30°[23].

Table S8 The $\Delta E_{\mathrm{nH_2O*}}$ and ΔSol of each ORR intermediate on sp-N1GDY/G with ice-like bilayer layer and five snapshots from AIMD, n is water number.

	$\Delta E_{\mathrm{nH_2O*}}$ (eV/H_2O)	n	ΔSol (2O*)	ΔSol (O*+OH*)	ΔSol (OOH*)	ΔSol (O*)	ΔSol (OH*)
Ice-like bilayer	-0.45(H-up)/ -0.46(H-down)	16	-0.31	-0.26	-0.32	-0.28	-0.27
AIMD-1	-0.43	18	-0.28	-0.28	-0.20	-0.27	-0.22
AIMD-2	-0.42	17	-0.26	-0.27	-0.26	-0.26	-0.21
AIMD-3	-0.41	17	-0.28	-0.28	-0.29	-0.28	-0.29
AIMD-4	-0.41	17	-0.23	-0.23	-0.28	-0.23	-0.26
AIMD-5	-0.43	19	-0.20	-0.20	-0.27	-0.20	-0.21
Average with 5 AIMD snapshots	—	—	-0.25	-0.25	-0.26	-0.25	-0.24

Table S9 The $\Delta E_{\mathrm{nH_2O*}}$ and ΔSol each ORR intermediate on Pyri-NGDY/G with ice-like bilayer layer and five snapshots from AIMD. n is the water number.

	$\Delta E_{\mathrm{nH_2O*}}$ (eV/H_2O)	n	ΔSol(OOH*)	ΔSol(O*)	ΔSol(OH*)
Ice-like bilayer	-0.45(H-up)/ -0.46(H-down)	16	-0.27	-0.45	-0.21
AIMD-1	-0.43	17	-0.20	-0.39	-0.21
AIMD-2	-0.44	17	-0.20	-0.40	-0.10
AIMD-3	-0.43	17	-0.23	-0.32	-0.13
AIMD-4	-0.43	17	-0.37	-0.37	-0.15
AIMD-5	-0.40	17	-0.31	-0.46	-0.33
Average with 5 AIMD snapshots	—	—	-0.26	-0.40	-0.18

Table S10 The adsorption Gibbs free energy of each ORR intermediate on sp-N1GDY/G, sp-N1GDY(OH)/G, and Pyri-NGDY/G with and without water using PBE+D2 functional.

	ΔG_{ads} (2O*)	ΔG_{ads} (O*+OH*)	ΔG_{ads} (OOH*)	ΔG_{ads} (O*)	ΔG_{ads} (OH*)
sp-N1GDY/G	2.57	1.38	—	0.70	-0.16
sp-N1GDY/G with water	2.24	1.06	—	0.40	-0.44
sp-N1GDY(OH)/G	—	—	4.23	2.18	0.97
sp-N1GDY(OH)/G with water	—	—	3.86	1.88	0.69
Pyri-NGDY/G	—	—	4.58	2.20	1.35
Pyri-NGDY/G with water	—	—	4.30	1.67	1.09

Table S11 The $\Delta E_{\mathrm{nH_2O*}}$ and the ΔSol of each ORR intermediate on sp-N1GDY/G and Pyri-NGDY/G with ice-like bilayer using PBE+D2 functional.

	$\Delta E_{\mathrm{nH_2O*}}$ (eV/H_2O)		ΔSol (2O*)	ΔSol (O*+OH*)	ΔSol (OOH*)	ΔSol (O*)	ΔSol (OH*)
	H-up	H-down					
sp-N1GDY/G	-0.56	-0.57	-0.33	-0.32	-0.37	-0.30	-0.28
Pyri-NGDY/G	-0.56	-0.57	—	—	-0.28	-0.53	-0.26

References:

[1] I. C. Man, H. Y. Su, F. C. Vallejo, H. A. Hansen, J. I. Martinez, N. G. Inoglu, J. Kitchin, T. F. Jaramillo, J. K. Nørskov. J. Rossmeisl, Universality in Oxygen Evolution Electrocatalysis on Oxide Surfaces. *ChemCatChem*, 2011, **3,** 1159-65.

[2] Q. Liang, G. Brocks, A. B. Hütter, Oxygen evolution reaction (OER) mechanism under alkaline and acidic conditions. *J. Phys. Energy,* 2021, **3,** 026001.

[3] C. J. Cramer. *Essentials of Computational Chemistry*, Second Edition. Wiley, 2004.

[4] D. R. Lide, CRC handbook of physics and chemistry, CRC Press, Boca Raton, USA, 2001, **76**,1995-1996.

[5] R. C. Weast, Handbook of chemistry and physics, Chemical Rubber Co., Cleveland, OH, 1971, C528-C529.

[6] J. Rossmeisl, A. Logadottir, and J. K. Nørskov, Electrolysis of water on (oxidized) metal surfaces, *Chem. Phys.* 2005, **319**, 178.

[7] J. K. Nørskov, J. Rossmeisl, A. Logadottir, L. Lindqvist, J. R. Kitchin, T. Bligaar, H. Jónsson, Origin of the Overpotential for Oxygen Reduction at a Fuel-Cell Cathode. *J. Phys. Chem. B*, 2004, **108**, 17886-17892.

[8] J. K. Nørskov, F. Studt, F. Abild-Pedersen, T. Bligaard, Fundamental Concepts in Heterogeneous Catalysis (New York, NY: Wiley), 2014.

[9] J. Li, H. M. Yin, X. B. Li, E. Okunishi, Y. L. Shen, J. He, Z. K. Tang, W. X. Wang, E. Yücelen, C. Li, Y. Gong, L. Gu, S. Miao, L. M. Liu, J. Luo, Y. Ding, Surface evolution of a Pt–Pd–Au electrocatalyst for stable oxygen reduction. *Nat. Energy,* 2017, **2**, 17111.

[10] R. Iftimie, P. Minary, M. E. Tuckerman, Ab Initio Molecular Dynamics: Concepts, Recent Developments, and Future Trends. *PNAS*, 2005, **102**, 6654-6659.

[11] M. Otani, O. Sugino, First-principles calculations of charged surfaces and interfaces: A plane-wave nonrepeated slab approach. *Phys. Rev. B: Condens. Matter Mater. Phys.*, 2006, **73**, 115407.

[12] S. Yoo, , Z. C. Xiao, S. X. Sotiris, On the phase diagram of water with density functional theory potentials: The melting temperature of ice Ih with the Perdew–Burke–Ernzerhof and Becke–Lee–Yang–Parr functionals. *J. Chem. Phys.,* 2009, 130, 221102-221104.

[13] Q. Yue, S. Chang, J. Kang, S. Qin, J. Li, Mechanical and Electronic Properties of Graphyne and Its Family under Elastic Strain: Theoretical Predictions, *J. Phys. Chem. C*, 2013, **117**, 14804-14811.

[14] G. F. Luo, X. M. Qian, H. B. Liu, R. Qin, J. Zhou, L. Z. Li, Z. X. Gao, E. G. Wang, W. N. Mei, J. Lu, Y. L. Li, S. Nagase, Quasiparticle energies and excitonic effects of the two-dimensional carbon allotrope graphdiyne: Theory and experiment. *Phys. Rev. B: Condens. Matter Mater. Phys.,* 2011, **84**, 075439.

[15] N. N.T. Pham, Nitrogen doping effects on the physical and chemical properties of bilayer graphdiyne: A density functional theory approach. *Applied Surface Science Advances*, 2022, **11**, 100301.

[16] W. Hu, T. Wang, R. Zhang, Jinlong Yang, Effects of interlayer coupling and electric fields on the electronic structures of graphene and MoS_2 heterobilayers. *J. Mater. Chem. C,* 2016, **4**, 1776-1781.

[17] M. Legesse, F. E. Mellouhi, E. T. Bentria, M. E. Madjet,T. S. Fisher, S. Kais, F. H. Alharbi, Reduced work function of graphene by metal adatoms. *Appl. Surf. Sci.* 2017, **394**, 98-107.

[18] Y. J. Yu, Y. Zhao, S. Ryu, L. E. Brus, K. S. Kim and P. Kim, Tuning the Graphene Work Function by Electric Field Effect. *Nano Lett.,* 2009, **9**, 3430-3434.

[19] F. Xu, K. Meng, B. Zhu, H. Liu, J. Xu, J. Yu, Graphdiyne: A New Photocatalytic CO_2 Reduction Cocatalyst. *Adv. Funct. Mater.,* 2019, **29**, 1904256.

[20] S. Pezzotti, A. Serva, F. Sebastiani, F. S. Brigiano, D. R. Galimberti, L. Potier, S. Alfarano, G. Schwaab, M. Havenith, M. P. Gaigeot, Molecular Fingerprints of Hydrophobicity at Aqueous Interfaces from Theory and Vibrational Spectroscopies. *J. Phys. Chem. Lett.* 2021, **12**, 3827-3836.

[21] A. K. Soper, F. Bruni, M. A. Ricci, Site–site pair correlation functions of water from 25 to 400 °C: Revised analysis of new and old diffraction data. *J. Chem. Phys.* 1997, **106**, 247-254.

[22] A. H. Narten, H. A. Levy, Liquid Water: Molecular Correlation Functions from X-Ray Diffraction. *J. Chem. Phys.* 1971, **55**, 2263-1971.

[23] A. Luzar, D. Chandler, Hydrogen-bond kinetics in liquid water. *Nature,* 1996*,* **379**, 55-57.